



King Saud University
Arabian Journal of Chemistry

www.ksu.edu.sa
www.sciencedirect.com



ORIGINAL ARTICLE

Synthesis of visible light driven TiO₂ coated carbon nanospheres for degradation of dyes

Waseem Raza ^a, M.M. Haque ^a, M. Muneer ^{a,*}, D. Bahnemann ^b

^a Department of Chemistry, Aligarh Muslim University, Aligarh 202002, India

^b Institut fuer Technische Chemie, Leibniz Universität Hannover, Callinstrasse 3, D-30167 Hannover, Germany

Received 27 June 2015; accepted 7 September 2015

KEYWORDS

Metal doped TiO₂;
CNS coated TiO₂;
Photocatalysis;
Dye degradation

Abstract Herein, we report the successful synthesis of visible light driven metal doped TiO₂ coated carbon nanospheres (CNS) via a facile hydrothermal approach. The synthesized materials were characterized by standard analytical techniques, such as XRD, SEM–EDS-mapping, TEM, FTIR, PL, Raman and UV–Vis absorption spectroscopy. The effect of dopants on the band gap energy, crystallite size and photocatalytic properties of the TiO₂ coated CNS was investigated systematically. The incorporation of dopants in TiO₂ matrix found to significantly extend the absorption edge toward visible region and efficient separation of charge carriers on excitation. The photodegradation of two different organic dyes were investigated to evaluate the activity of the photocatalyst under different conditions such as dopant percentage, catalyst dose, different quenchers and calcination temperature. The best photocatalytic activity was observed with 3.0% Ce, doped TiO₂ coated CNS with 1.5 g L⁻¹ concentration calcined at 400 °C. We also performed the antibacterial activity of pure and doped-TiO₂ coated CNS against pathogenic gram negative and gram positive bacteria. The doped-TiO₂ coated CNS exhibited excellent antibacterial activity against both bacteria.

© 2015 The Authors. Production and hosting by Elsevier B.V. on behalf of King Saud University. This is an open access article under the CC BY-NC-ND license (<http://creativecommons.org/licenses/by-nc-nd/4.0/>).

1. Introduction

From the past few decades the rampant use of pharmaceutical, pesticide, industrial chemicals and different type of dyes in

cosmetic, paper and leather is well known. A large amount of pollutants are disposed continuously into water bodies from above sources, which lead to undesirable accumulation of toxic components leading to serious environmental problems (Daghrir et al., 2013). Therefore, it is advisable to look for an economical and feasible technique for remediation of such hazardous environmental effluents (Anil Kumar Reddy et al., 2010). Advanced oxidation processes (AOPs) have been proved as an excellent method for the degradation of environmentally hazardous material (Daghrir et al., 2013). Photocatalysis is the advanced oxidation processes (AOPs) and received much more attention for the degradation of pollutants in aqueous phase by simple and efficient manner (Akpan and

* Corresponding author. Tel.: +91 571 2700920x3365.

E-mail addresses: m.muneer.ch@amu.ac.in, readermuneer@gmail.com (M. Muneer).

Peer review under responsibility of King Saud University.



Production and hosting by Elsevier

<http://dx.doi.org/10.1016/j.arabjc.2015.09.002>

1878-5352 © 2015 The Authors. Production and hosting by Elsevier B.V. on behalf of King Saud University.

This is an open access article under the CC BY-NC-ND license (<http://creativecommons.org/licenses/by-nc-nd/4.0/>).

Please cite this article in press as: Raza, W. et al., Synthesis2 coated carbon nanospheres → of visible light driven TiO₂ coated carbon nanospheres for degradation of dyes. Arabian Journal of Chemistry (2015), <http://dx.doi.org/10.1016/j.arabjc.2015.09.002>

Hameed, 2009; Singh et al., 2007). Among various semiconductors, TiO₂ is one of the most efficient photocatalyst for degradation of pollutants owing to its enormous advantages including its high catalytic activity, good chemical inertness, nontoxicity, low cost and strong chemical stability in a large pH range (Haque and Muneer, 2007; Martins et al., 2014; Zhong et al., 2010). However, the use of TiO₂ for industrial application is restricted due to (i) its wide band gap (3.2 eV for anatase), therefore, it absorbed only UV light and limit the effective usage of solar light (3–5%), and (ii) fast recombination rate of photogenerated electron and hole pairs (Habib et al., 2013; Yu et al., 2011).

Recently, hollow nanospheres have received greater attention due to their unique structural feature, wide application in catalysis, magnetic, chemical, electrical and optical fields. Various methods have been developed for the synthesis of nanospheres (Zhang et al., 2009a). Nanospheres also received greater attention in the field of photocatalysis due to their high specific area, low density, porous structures and better catalytic activity (Guo et al., 2009; Li et al., 2013; Wheeler et al., 2010). The presence of carbonaceous material such as carbon nanospheres may facilitate the enhanced photocatalytic performance through providing high surface area, highly adsorptive active sites, photosensitization, band gap tuning and decrease in the electron hole recombination rate (Titirici, 2013). The carbonaceous material increases the adsorption of the dye and provides good contact between the dye and the photocatalyst. The carbon nanospheres play an important role in improving the photocatalytic activity of TiO₂ under UV light source by yielding synergistic effects between TiO₂ and carbonaceous material. Few investigators report that carbonaceous material can efficiently capture and transport the photo-generated electrons due to their high conductive activity (Xia et al., 2014).

Up to date, much efforts have been carried out to extend the spectral response of photocatalyst into visible region for photodegradation of pollutants in various ways, including doping with metals, nonmetals, rare earth metals and coupling with other semiconductor (Chand et al., 2013; Chowdhury et al., 2012; Gomez et al., 2012; Gurkan et al., 2013; Nahar et al., 2006; Rehman et al., 2009; Rosario and Pereira, 2014; Wang et al., 2014, 2005; Schneider et al., 2014). Doping of TiO₂ with transition and rare earth metal have received much attention for improving the photocatalytic activity due to vacant d and f orbitals. Among various transition metal ions, Mn²⁺ received more attention than other transition metal ion due to similarity in ionic radii of Mn²⁺ and Ti⁴⁺. Therefore introduction of Mn²⁺ ion into the TiO₂ lattice is easier than other transition metals. The incorporation of Mn²⁺ easily produces oxygen vacancy without causing significant distortion in the crystal structure of TiO₂. The trapping of electron by Mn²⁺ is temporary because it has stable d⁵ configuration. Thus it can easily transfer the temporarily trap electron to absorbed O₂ to enhance the photocatalytic activity for photodegradation of targeted pollutants (Zhu et al., 2006). In addition the d-orbital of Mn²⁺ ion may overlap with the conduction band of TiO₂ and thus leading to reduction in band gap. The formation of impurity band by doping of metal in TiO₂ lattice is an another approach to extend the spectral response toward visible region, resulting in the absorption of more visible light. Therefore, photocatalytic activity of doped materials enhanced for degradation of dyes (Wang et al.,

2010a). Among various rare earth metals Ce ion also received much attention because of its redox coupling between Ce³⁺/Ce⁴⁺ and having good oxygen storage and transport capacity. It contains ability to shift between Ce₂O₃ and CeO₂ under reducing and oxidizing conditions (Song et al., 2008; Yu et al., 2010). The electron scavenging capacity of Ce is good and it can easily trap the electron. The trapped electrons by Ce are subsequently transferred to the adsorbed O₂, hence extending the lifetime of the electron–hole pair. The Ce ion gets transferred to crystal surfaces due to the size dissimilarity with Ti⁴⁺ ions (Zhang et al., 2009b).

Nasir et al. have reported the photocatalytic activities of TiO₂ doped with Ce and S ions for the degradation of Acid Orange 7 (100%, 5 h) under visible light irradiation (Nasir et al., 2013). Jaimy et al. have also reported the synthesis of Fe and Ce doped and codoped TiO₂ and effect of doping with different metal ions into the TiO₂ lattice for the decomposition of Methylene Blue (74%, 160 min) under visible light illumination (Jaimy et al., 2012). Recently, Ozmen et al. synthesized the nano-sized Mn-doped TiO₂ using sol gel method for degradation of different xenobiotics under visible irradiation (Ozmen et al., 2015). Cacho et al. studied on photo-induced NO removal by Mn-doped TiO₂ under indoor-light illumination conditions. They have reported 95% degradation of NO after 6 h (Cacho et al., 2011). On the other hand Kuyumcu have reported the removal of different dyes by using M/TiO₂ (M = Cu, Ni, Co, Fe, Mn and Cr) photocatalysts under visible light irradiation and 16.41% and 26.18% degradation of Methylene blue and Methyl orange takes place after 5 h (Kuyumcu et al., 2015).

Besides these considerations, the antibacterial studies of fabricated nanospheres were also been carried out (Pan et al., 2014; Xu et al., 2004). Matsunaga et al. performed an experiment against antimicrobial cell using a Pt doped-TiO₂ in water irradiation with near-UV light for 120 min (Matsunaga et al., 1985). Extensive research has been carried out by using TiO₂ against bacteria. However, the overall antibacterial activity of pure TiO₂ is not good in comparison with doped TiO₂ (Josset et al., 2008). The antibacterial activity depends on various factors such as crystalline structure, surface area, recombination of photogenerated charge carrier, concentration and synthesis methodology (Gogoi et al., 2006; Rincón and Pulgarin, 2003). The doped TiO₂ nanoparticles have advantage over pure TiO₂ because doped TiO₂ nanoparticles neutralize most of the pathogenic microorganisms as compared to pure TiO₂ (Zhang et al., 2010); thus, doped titania revealed enhanced antibacterial activity.

This paper deals with synthesis of Ce and Mn doped TiO₂ coated carbon nanospheres (CNS) with a uniform morphology and good structural stability by hydrothermal method using carbon spheres as support followed by an annealing treatment and characterized using standard analytical techniques. The photocatalytic activities of the synthesized material were tested for the degradation of two different chromophoric dye derivatives such as Acid Yellow 29 (azo dye) and Acid Green 25 (anthraquinone dye) under visible light illumination as a function of irradiation time in aqueous suspension in an immersion well photochemical reactor with a 500 W tungsten halogen linear lamp in the presence of atmospheric oxygen. We also evaluated the antibacterial activity of the fabricated nanospheres against the gram positive and gram negative bacteria.

2. Experimental

2.1. Reagents and chemicals

Analytical grade titanium oxysulfate and dye derivatives, Acid Yellow 29 (AY-29) and Acid Green 25 (AG-25) were obtained from Sigma–Aldrich while glucose was obtained from Merck. Ammonium ceric nitrate was purchased from Central Drug House, India. Manganese (II) sulfate monohydrate was purchased from Himedia Laboratories Pvt. Ltd. The water used in all experiments was double distilled. All cultures were taken from the departmental culture collection.

2.2. Material preparation

2.2.1. Synthesis of carbon nanosphere (CNS)

In a typical procedure, (3.96 g) glucose was dissolved in 80 ml double distilled water in a round bottom flask and magnetically stirred for 30 min to form a homogeneous solution at room temperature and then transferred into 100 ml Teflon-lined stainless steel autoclave. The autoclave containing the raw material was sealed tightly and put in electric muffle furnace. The temperature of an electric muffle furnace (hydrothermal) was maintained at 180 °C for 8 h. The black precipitate was obtained after cooling the autoclave naturally at room temperature and then washed thoroughly with water and ethanol. Then the obtained product was dried at 80 °C for 5 h. Finally we get blackish brown solid identified as CNS (Li et al., 2011).

2.3. Characterization

X-ray diffraction (XRD) analysis of all the prepared sample were performed by using Rigaku Miniflex II diffractometer in 2θ range of 20–80° with Cu K α radiations ($\lambda = 1.5418 \text{ \AA}$) operated at voltage of 40 kV and current of 15 mA with scanning speed of 2.0° per min for examining crystal structure, phase composition and crystallite size. The surface morphology and elemental analysis of the as prepared material after calcination were examined by scanning electron microscope (JEOL) JSM-6510 coupled with EDS & mapping and transmission electron microscope, (JEOL) JEM-2100). UV–Vis spectrum was recorded at room temperature using Shimadzu UV–Vis spectrophotometer (Model 1601). Fourier transform infrared (FTIR) spectrum of the fabricated sample was recorded in KBr powder using a Perkin-Elmer (FT-IR Spectrum Frontier). The Raman spectrum was taken using Varian FT-Raman spectrometer. Signals were got upon excitation of the materials by a red diode laser. The room-temperature photoluminescence (PL) spectrum of the fabricated material was recorded using Hitachi (F-2700). A Xe lamp was used as excitation source during PL study at an excitation wavelength 280 nm.

2.4. Antibacterial activity

The antibacterial activity of fabricated pure and doped TiO₂ coated CNS was studied against *Streptococcus pyogenes* (Clinical isolate), *Staphylococcus aureus* (ATCC-29313), *Pseudomonas aeruginosa* (ATCC-27853) and *Escherichia coli*

(ATCC-25922) bacteria. The nutrient broth culture was prepared in water by mixing (4.0 g) peptone, (4.0 g) NaCl, (4.0 g) agarose gel powder and (1.0 g) yeast extract. The mixture was sterilized in an autoclave at 120 °C for 30 min and then poured into separate petri dishes after cooling at room temperature. Culture of bacteria was inoculated in 20 ml nutrient broth, incubated for 24 h at 37 °C and centrifuged at 3000 rpm for 7 min. Prior to studied, the bacterial solution diluted to 10⁹ times using 0.9% NaCl solution to get about 100–200 colonies on the petri dish. Diluted bacterial culture (2 ml) of an approximate concentration of 10⁷ colony forming units per milliliter (CFU/ml) was spread on the pure and doped TiO₂ coated petri dish and incubated at 37 °C for 24 h. The formed bacterial colonies were counted by a viable count method.

2.5. Photocatalytic activity

The photocatalytic activity of the synthesized materials were evaluated by studying the degradation of two different chromophoric dyes such as AY-29 and AG-25 in aqueous suspension under visible light irradiation. An immersion well photochemical reactor made of Pyrex glass was used for all photocatalytic experiments. For irradiation experiment, a tungsten halogen linear lamp (500 W, 9500 Lumens) was used as visible light source ($\lambda \geq 400$). In order to maintain the photoreactor temperature ($20 \pm 0.5 \text{ }^\circ\text{C}$) constant the refrigerated water circulation was used. For a typical photocatalytic experiment an aqueous solution of dye (200 ml) was taken into the reactor and the appropriate amount of photocatalyst (Ce and Mn doped TiO₂ CNS) was added. Prior to irradiation, the suspension was stirred magnetically for at least 30 min in the dark in order to allow the system to reach equilibrium; the loss of dye due to adsorption/desorption can be taken into account. After that the suspension was exposed to light. The suspension bubbled with atmospheric oxygen with an air pump to ensure a constant supply of oxygen. The suspension (5 ml) was collected before and after at regular interval during the irradiation and centrifuge before analysis to remove photocatalyst powder. The degradation of dye derivatives was monitored using UV–Vis spectrophotometer at their λ_{max} . The degradation ratio (η) was calculated by Eq. (1) as given below:

$$\eta = \frac{C_0 - C}{C_0} \times 100\% \quad (1)$$

where C_0 is initial concentration and C is concentration at particular time (t).

3. Results and discussion

3.1. UV–Vis absorption spectra

The UV–Visible absorption spectra of pure and doped TiO₂ coated CNS were measured to study the optical response of doped TiO₂ coated CNS and shown in Fig. 1 (A and B). The UV–Vis absorption spectroscopy is a good technique, which determines the light absorbing capacity of the as prepared material (Barpuzary and Qureshi, 2013; Chaturvedi et al., 2015). The band gap energy of synthesized powder plays an important role in deciding the photocatalytic activity of semiconductor photocatalyst. The band gap energy of pure and

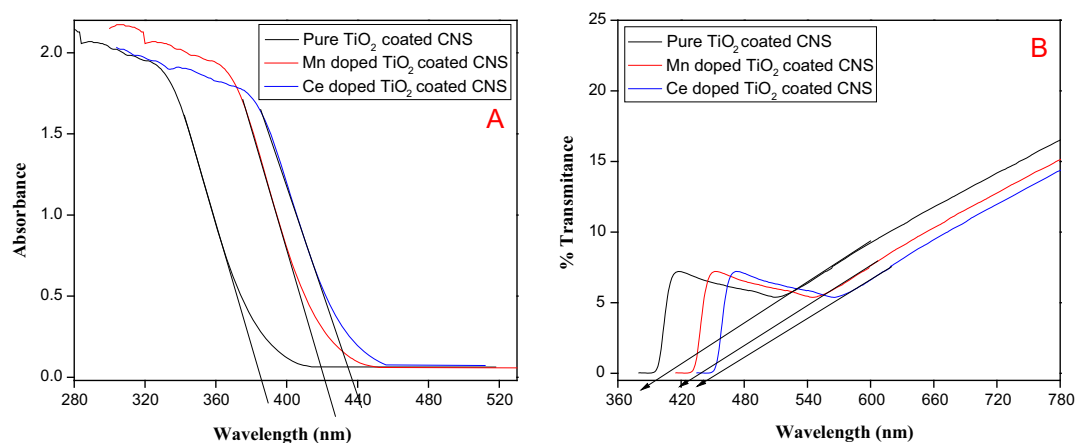


Figure 1 (A) Absorption spectra and (B) optical transmission spectra of pure and Ce/Mn doped TiO₂ coated CNS.

doped TiO₂ particle was calculated from the wavelength obtained from UV–Vis absorption spectra using the following Eq. (3) (Štengl et al., 2009):

$$\text{Band gap energy (eV)} = \frac{1240}{\text{Wavelength (nm)}} \quad (2)$$

The valence band of TiO₂ is made up of 2p orbital of oxygen and the conduction band edge derives from 3d orbital of Ti. The incorporation of metal ions may result formation of impurity level between VB and CB which leads to the shifting of fundamental absorption edge at the longer wavelength (i.e. red shift). This indicates that doping can shift the absorption of TiO₂ coated CNS toward visible region; leading to decrease in band gap energy compared to pure TiO₂ (Štengl and Bakardjeva, 2010; Štengl et al., 2009). The impurity level either accepts an electron from the valence band or can donate an electron to the conduction band. Now the distance between impurity level and valance band or conduction is reduced. Thus visible light becomes energetic enough to facilitate the electron transition. The dopant also traps electrons and therefore reduced the rate of recombination of e⁻/h⁺ pair. Thus photocatalytic activity of doped TiO₂ greatly enhanced for photodegradation of targeted pollutants. Similar results and mechanism were also reported by other workers. The results suggested the narrowing in band of doped TiO₂ due to formation of impurity band. The presence of Ce/Mn ions shift the wavelength edge toward visible region beside this, it can also improve the physical properties of TiO₂ coated CNS, such as control the crystallite size, helped in producing larger surface area and suppressed the phase transformation from anatase to rutile (CAI et al., 2008). At higher dopant concentration an increase in band gap energy was observed as observed in our earlier studies (Raza et al., 2015a, 2015b). At high dopant percentage the blocking of light rays or shadowing effect was observed. The turbidity of powder takes place due to aggregation of the catalyst particles, which decreases the penetration depth of light. The aggregation of TiO₂ coated CNS powder cover the part of photosensitive surface thereby decreasing the number of surface active sites (Devi et al., 2009; Li et al., 2001; Ni et al., 2007). For efficient photodegradation of dyes optimum catalyst loading should be maintained to ensure total absorption of photons and maximum adsorption of the dye molecules. The fabricated pure, Mn and Ce-doped TiO₂

photocatalysts showed the absorption at 385, 422 and 438 nm corresponding to band gap energies of 3.22, 2.94 and 2.83 respectively.

3.2. Photoluminescence (PL) spectra

The PL spectra study is a good technique which received great attention in the field of photocatalysis and a useful probe for understanding the separation efficiency of photogenerated electrons and holes. The PL spectra originate from the recombination of excited electrons and holes, a higher PL intensity indicates a higher recombination rate of electron hole and lower separation of charge carrier and lower intensity exhibits lower recombination rate and higher separation efficiency of photogenerated e⁻/h⁺ pairs. To investigate the effect of dopants on the charge separation of photogenerated e⁻/h⁺ pairs, we measured PL spectra in the range of 500–600 nm under the excitation of 280 nm wavelength. The PL spectra of pure and doped TiO₂ coated CNS are similar and show broad and strong PL signals in the region of 525–560 nm (Fig. 2). The PL emission intensity of doped TiO₂ coated CNS was lower than pure TiO₂ coated CNS which indicates that efficiency of charge separation was higher and recombination rate was lower than pure TiO₂ coated CNS. The dopant acts as electron-trapping agent and thus promotes electron and hole separation and transfer effects. The photocatalytic activity of doped TiO₂ coated CNS was found to be higher than pure TiO₂ coated CNS and this may be attributed to higher separation of charge carrier. However, the PL intensity of Ce doped TiO₂ coated CNS is lower than pure and Mn TiO₂ coated CNS doped indicated higher charge separation and greater reduction in recombination. Thus photocatalytic activity of Ce doped TiO₂ coated CNS was found to be higher than pure and Mn doped TiO₂ coated CNS.

3.3. Size and morphology of synthesized CNS (SEM–EDX-mapping and TEM)

The surface morphology of pure and doped TiO₂ coated CNS was examined by using scanning electron microscopy (SEM) coupled with EDS and mapping and transmission electron microscopy (TEM) analysis. The SEM images of CNS at

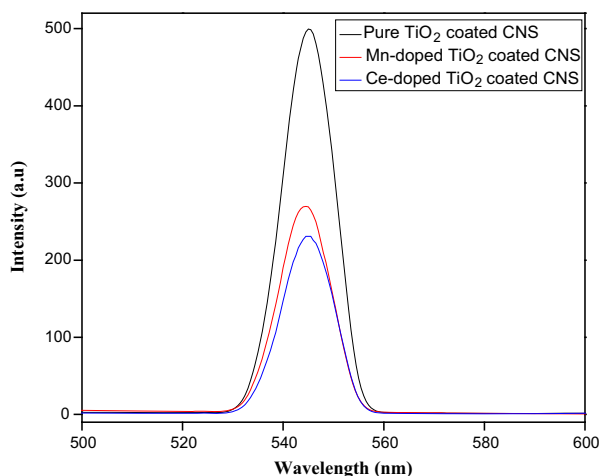


Figure 2 PL spectra of pure and Ce/Mn doped TiO₂ coated CNS.

different magnification revealed that the pure and doped TiO₂ coated CNS was spherical in shape (Fig. 3S(A–D), SI). The pure and doped TiO₂ coated CNS made up aggregation of spherical granules, but the obvious differences can be found in their morphologies. The average size of carbon spheres and pure TiO₂ coated CNS was found to be 60–96 nm and the size of doped TiO₂ coated CNS remained 20–30 nm. The doping of Ce and Mn with different concentration leads to decrease the grain size and some change in surface morphology, implying the deposition of Ce and Mn. Metal ions also

decrease the aggregation of CNS which leads to increase the surface area and therefore increase in the photocatalytic reaction sites. Hence, photocatalytic activity of doped material was found to be increased for degradation of target pollutants.

In order to investigate the presence of different metal ions, percentage of dopant and geometrical distribution of atoms, energy-dispersive X-ray (EDX) spectroscopy coupled with elemental mapping was carried out. The EDX and element mapping results indicate that C, Ce and Mn are present in the CNS and the distribution of Ce and Mn is highly uniform in the TiO₂ particle over the entire volume of the spheres (Figs. 4S and 5S, SI). The atomic ratio of Ce and Mn measured from EDX and found to be 2.72% and 1.31%, which is very close to experimental value.

The surface morphology and structural characterization of doped TiO₂ coated CNS were further analyzed by Transmission electron microscopy (TEM) as shown in Figs. 3 and 4. TEM images of prepared CNS display good crystal structure and particles exhibit spherical shape. It can be seen from the figs that the average particle size of doped CNS was found to be 11.18 nm. The dark black spot indicates the presence of heterojunction or distribution of carbon and metals on the surface of TiO₂.

3.4. Antibacterial activity

The antibacterial activity of pure and doped TiO₂ coated CNS (Ce-3.0% and Mn-1.5%) was investigated against gram positive [*S. aureus*, *S. pyogenes*] and gram negative [*P. aeruginosa*, *E. coli*] bacteria and the result was compared with the standard

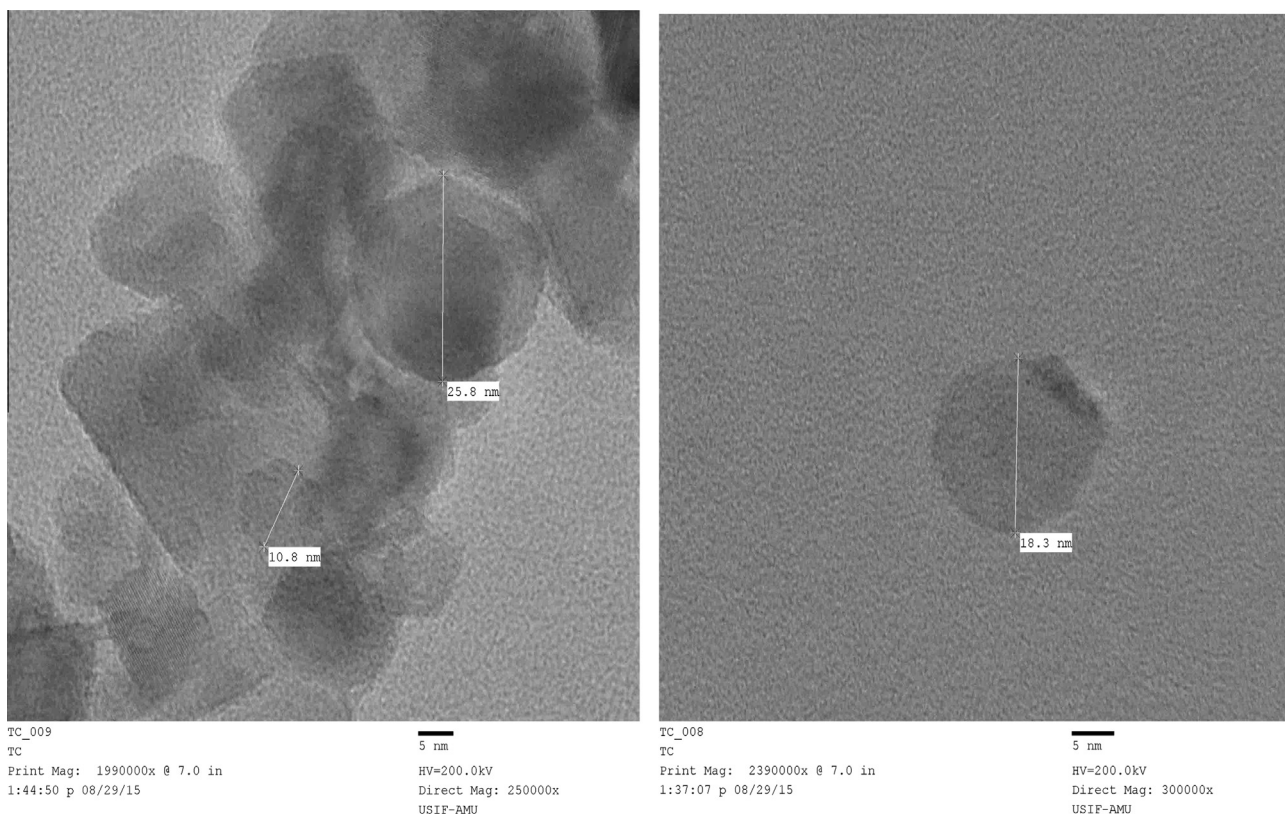


Figure 3 TEM image of Ce-doped TiO₂ coated CNS.

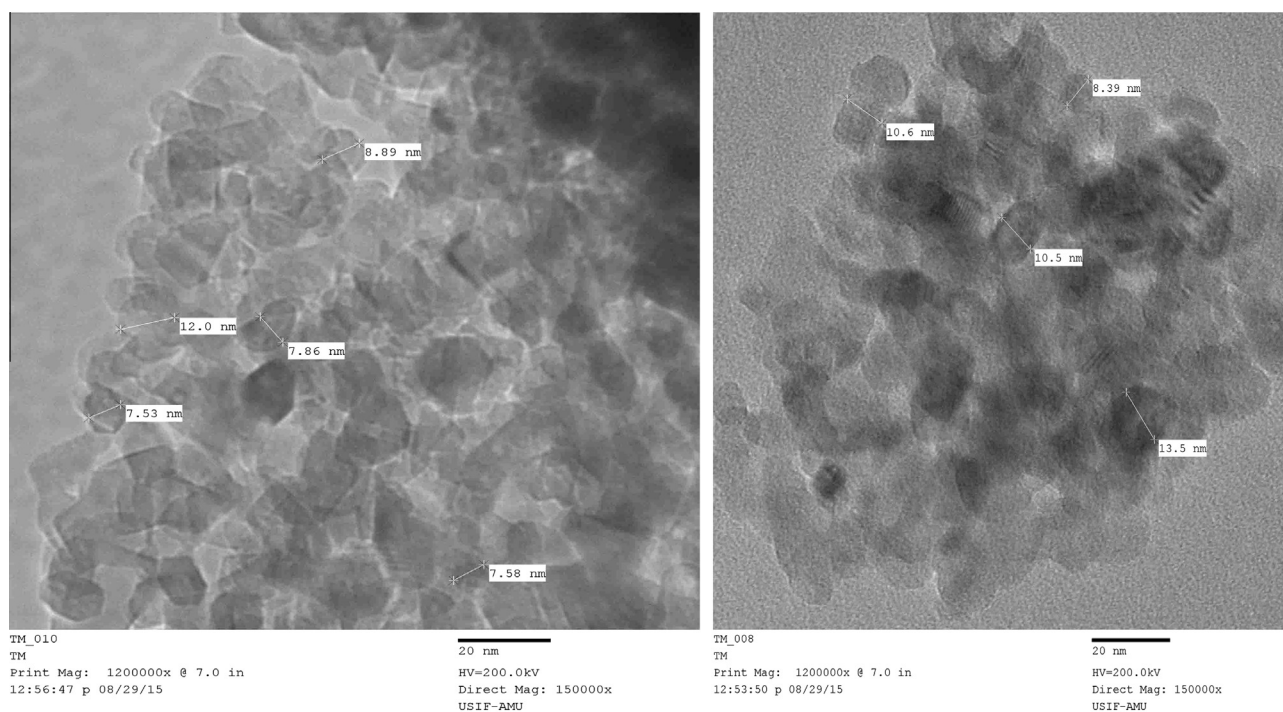


Figure 4 TEM image of Mn-doped TiO₂ coated CNS.

drug “Ciprofloxacin”. The results indicate that the fabricated materials have better antibacterial activity against both Gram-negative and Gram-positive bacteria. The gram negative bacteria showed higher resistance than gram positive bacteria toward the fabricated materials. The outer covering of gram negative bacteria made up of a thin layer of peptidoglycan and more complex cell wall with two membranes a plasma membrane and an outer membrane. However, the outer covering of gram positive bacteria composed of many layers of peptidoglycan and only one membrane (plasma membrane). Therefore, the outer membrane of gram negative bacteria influences the permeability of many molecules and makes it to resist. The cell wall of bacteria has negative charge. The presence of negative charge at the surface of gram positive bacteria due to teichoic acid linked to either the peptidoglycan or the underlying plasma membrane. However, the outer membrane of gram negative bacteria composed of phospholipids and lipopolysaccharides. The lipopolysaccharides impart a strong negative charge on the surface of gram negative bacterial cells. During photocatalytic process of pure and doped TiO₂ CNS highly reactive species such as superoxide radical anions, hydroxyl radical and hydrogen peroxide were produced. The suppression of bacterial growth by pure and doped TiO₂ was well known by the generation of reactive species such as $\cdot\text{OH}$, $\cdot\text{O}_2^-$ and H_2O_2 (Jiang et al., 2010; Shakir et al., 2014). Among all reactive species the short lived hydroxyl radical is highly reactive. The negatively charged superoxide radical anions do not penetrate the cell membrane. Hydrogen peroxide is less harmful but can enter the cell. The results indicate that the doped TiO₂ nanoparticles showed higher antibacterial activity than pure TiO₂. This is due to the fact that doping of metal on the surface of TiO₂ decreases the recombination rate of charge carrier and increase the charge separation (Wang et al., 2011), which increase the lifetime of charge carrier by

splitting the arrival time of photogenerated electrons and holes to reach the surface of photocatalyst. Therefore electron and hole easily take part in the formation of highly oxidizing (hydroxyl radical) and reducing (superoxide radical anion) agent, which increases the antibacterial activity of doped particles. The Ce doped TiO₂ showed higher antibacterial activity than pure and Mn doped TiO₂ because of the high surface area, much decrease in recombination rate of photogenerated charge carrier and good crystal structure. Another region was the formation of more reactive species in case of Ce than Mn-doped TiO₂ coated CNS due to more electron scavenging capacity of Ce than Mn. The percent area of inhibition by pure and doped TiO₂ was plotted against all bacteria and compared with standard drug Ciprofloxacin (Fig. 5).

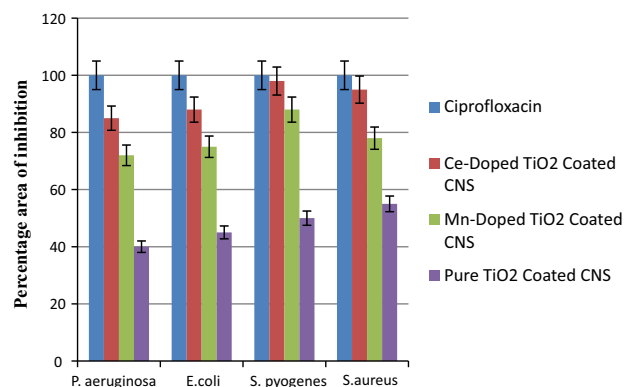


Figure 5 Antibacterial activity of pure and Ce/Mn doped TiO₂ coated CNS and ciprofloxacin against gram negative and gram positive bacteria.

3.5. Evaluation of photocatalytic activity

The photocatalytic performance of Ce and Mn doped TiO₂ coated CNS was studied for the degradation of two different organic dyes (AY-29 and AG-25) under visible light illumination. Photocatalytic degradation was also examined at different catalyst loading; different calcination temperature, different dopant concentration (SI) and different scavengers for getting optimal condition for best degradation. The stability (SI) of Ce and Mn doped TiO₂ CNS was examined by the reuse of catalyst for the degradation of dyes. The used catalyst washed with acetone and water, dried in an oven and calcined at 400 °C in the electric muffle furnace for 30 min.

The photocatalytic activity of the as prepared photocatalysts (3.0% Ce doped TiO₂ CNS, calcination temperature 400 °C and catalyst loading 1.5 g l⁻¹ and 1.5% Mn doped TiO₂ coated CNS, temperature 400 °C and catalyst loading 2 g l⁻¹) were evaluated by monitoring the degradation of two different chromophoric dyes such as AY-29 and AG-25 in an aqueous suspension under visible light irradiation. The degradation of dyes were investigated by measuring the change in the absorbance as a function of irradiation time in the presence of 3.0% Ce and 1.5% Mn doped TiO₂ coated CNS. There is almost no change in the absorbance of AY-29 and AG-25 under visible light illumination without photocatalyst. Therefore, both dyes were stable and do not reveal self-photodegradation under visible light irradiation without catalyst. Hence, AG-25 and AY-29 can only be decomposed under the joint function of light and catalyst. Figs. 8S and 9S, (SI) shows the change in the concentration as a function of irradiation time in the presence of different concentration (0–4.0%) of Ce and (0–2.0%) Mn doped TiO₂ CNS. Inset Figs. 8S and 9S, (SI) display the change in the absorbance at different time intervals on irradiation of AY-29 and AG-25 in the presence of 3.0% Ce and 1.5% Mn doped TiO₂ coated CNS respectively. The results indicate that 90% and 77% degradation of AY-29 and AG-25 dyes takes place after 120 min irradiation time in the presence of Ce (3.0%) and Mn (1.5%) doped TiO₂ coated CNS respectively. It could be seen from the figs that the decrease in absorption of both dyes takes place (406 & 640 nm) as irradiation time increases. The color of the dye solution became lighter as the irradiation time increased due to gradual degradation of chromophoric group present in the dyes.

To establish the activity of synthesized catalyst, we also performed the experiments for decomposition of two different chromophoric dyes such as AY-29 and AG-25 at optimal condition in the presence of Ce and Mn-doped TiO₂ coated CNS with different concentration of Ce and Mn under visible light illumination with continuous purging of atmospheric oxygen. Fig. 6 (A and B) shows the degradation rate of AY-29 and AG-25 in the presence of doped and undoped TiO₂ coated CNS. The results indicate that the degradation rate of the all the dye derivatives were found to increase with increase in dopant concentration up to certain limit and then decrease in degradation rate was observed, whereas in the presence of pure TiO₂ coated CNS no observable degradation of the dyes could be seen under visible light illumination. Similar results were also observed in other papers (Haque et al., 2014; Paul et al., 2010; Raza et al., 2014; Raza et al., 2015a, 2015b). The results indicate that the decolorization of AG-25 was found to be lower than AY-29 due to presence of stable and bulky aromatic rings which suppress the interaction between catalysts and dye. The adsorption of AG-25 was lower than AY-29 on the surface of catalyst which decrease photocatalytic degradation of AG-25 as compared to AY-29.

For better understanding of decomposition of dyes by prepared materials, the kinetic study was performed under optimum condition. The kinetic study for degradation of dyes plays an important role for computing the efficiency viability of dye derivatives in wastewater (Li et al., 2012). The photocatalytic degradation of dyes containing pure, Ce and Mn doped TiO₂ CNS were evaluated by using well known Langmuir–Hinshelwood kinetic model. It was found that photodegradation rate of dyes obeys pseudo-first-order rate. Similar results have been reported earlier (Ganesh et al., 2012; Wang et al., 2011). The rate was calculated using following Eq. (3):

$$\ln(C_0/C) = kt \quad (3)$$

where C_0 is concentration at time t_0 , C is concentrations at particular irradiation time and k is rate constant. The rate constant (k) for both dyes were calculated from the slopes of straight line obtained from the plot of natural logarithm $\ln(C)$ vs. irradiation time (t) as shown in Fig. 7 (A and B). The variations in $\ln(C_0/C)$ as a function of irradiation time for AG-25 and AY-29 are given in Figs. 8 and 9 [Ce/Mn-doped, A (0–10 min, B 10–120 min)]. From these figs it was observed

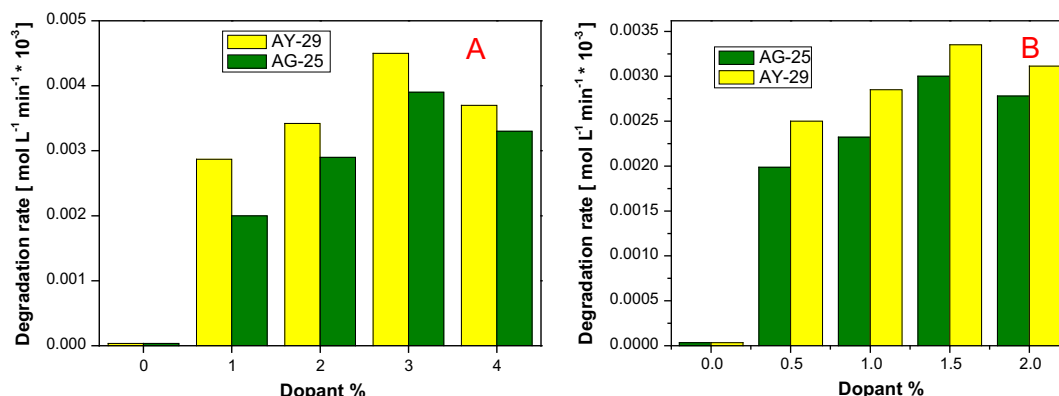


Figure 6 (A) Photocatalytic degradation of AY-29 and AG-25 in the presence of Ce-doped TiO₂ coated CNS (with varying concentration) under visible light illumination. (B) Photocatalytic degradation of AY-29 and AG-25 in the presence of Mn-doped TiO₂ coated CNS (with varying concentration) under visible light illumination.

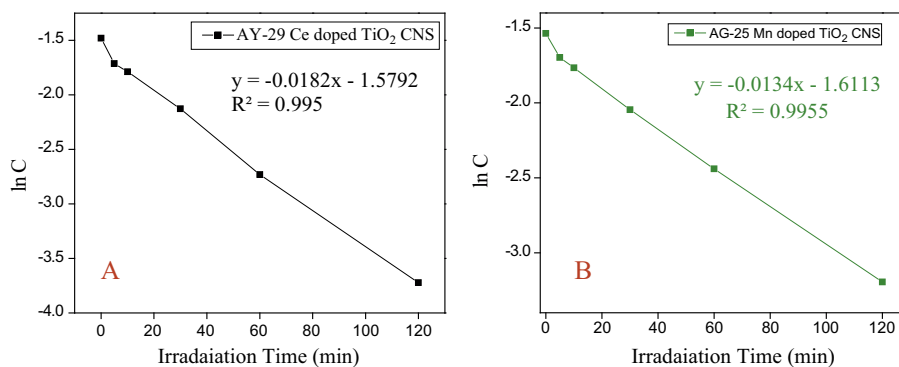


Figure 7 (A and B) The plot of $\ln C$ vs. irradiation times depicting the dye photodegradation follows pseudo 1st order kinetics.

that the degradation rate of dyes increases with increase in dopant concentration up to 3.0% in case of Ce and 1.5% in case of Mn and then decreases.

The increase in the photocatalytic activity by increasing the dopant concentration from 1% to 3.0% (Ce) and 0.5% to 1.5% (Mn) may be due to the shortening of the band gap by introducing new energy level also known as impurity band between the conduction band and valence band of TiO_2 . Therefore, TiO_2 has been activated under visible light illumination. This impurity band can either accept electrons from the valence band or donate electrons to the conduction band. After formation of new band between VB and CB the band gap energy decreases therefore, longer wavelength i.e. visible light enough energetic to facilitate the electron transition. Another reason for the increase in the photocatalytic activity by increasing the dopant concentration could be attributed to the fact that the doping of TiO_2 with Ce or Mn introduces new trapping sites which affects the lifetime of charge carriers by splitting the arrival time of photogenerated electrons and holes to reach the surface of photocatalyst and thus electron-hole recombination is reduced. It can be explained on the basis of the results that the dopant can act as electron-hole separation centers. Nevertheless, further increase in concentration of dopant leads to decrease in degradation of dyes. At higher dopant concentration 4.0% (Ce) and 2.0% (Mn) there was occurrence of multiple trapping of charge carriers and hence the possibility of electron-hole recombination increases and fewer charge carriers will reach the surface to initiate the degradation of the dye. Therefore, decrease in decomposition of dyes was observed (Wang et al., 2011, 2010b). In addition at high dopant percentage the blocking of light rays or shadowing effect was observed. The turbidity of powder takes place due to aggregation of the catalyst particles, which decreases the penetration depth of light. The aggregation of TiO_2 coated CNS powder covers the part of photosensitive surface thereby decreasing the number of surface active sites. Only appropriate amounts of dopant can improve the photocatalytic activity of nanospheres.

The results suggest that the presence of Ce and Mn metal ions in TiO_2 matrix extends the visible light absorption capacity because of narrowing of the band gap due to the formation of impurity band which greatly inhibits the recombination rate of photogenerated charge carrier and plays an important role in enhancing the photocatalytic performance of TiO_2 coated CNS for decomposition of absorbed pollutants. However,

the photocatalytic activity of Ce doped TiO_2 is much higher than pure and even Mn-doped TiO_2 coated CNS. This may be due to that the surface of Ce^{4+} doped TiO_2 coated CNS has higher affinity for adsorption of chemical species containing unpaired electrons and dyes due to presence of much higher Lewis surface acidity of Ce^{4+} doped TiO_2 coated CNS and rough surface. Rather, the Ce doped TiO_2 coated CNS has high crystalline state and larger surface area. Photocatalytic activity of titania also depends upon crystallinity, which decreases with increase in Ce doping more than Mn doping (Zhang et al., 2009b). Due to good Lewis surface acidity of Ce ions it can form complexes with various Lewis bases including amines, organic acids, alcohols, thiols and aldehydes (Ranjit et al., 2001). Therefore, adsorption of more organic pollutants occurs on the surface of semiconductor by doping of Ce ion. The doping of Ce^{4+} restrains the crystal growth, matrix distortion, crystal expansion and retards the recombination of the photoexcited e^-/h^+ pairs. The higher photocatalytic activity of Ce-doped TiO_2 may also be attributed that Ce exhibits two oxidation, namely +3 and +4, which have the ability to shift between CeO_2 and Ce_2O_3 under oxidizing and reducing condition (Song et al., 2008; Yu et al., 2010). The doping with Ce can permit the absorption of more visible light due to formation of impurity level attributed to shorting of distance between VB and CB of TiO_2 more in case of Ce than Mn. The electron scavenging capacity of Ce^{4+} was found to be better than Mn^{2+} due to presence of vacant f orbital. Therefore, Ce^{4+} cation can easily trap excited electrons (Eq. (4)) and CeO_2 has high storage and transport capacity for oxygen (Sreeremya et al., 2012). Hence, formation of more labile and highly mobile species of oxygen takes place during Ce doping. Thus the electrons trapped in the $\text{Ce}^{4+}/\text{Ce}^{3+}$ site can easily be transferred to the surrounding adsorbed oxygen to form super oxide species (O_2^- {Eq. (5)}), hence extending the lifetime of the electron-hole pair by reducing the recombination of charge carriers (Zhang et al., 2009b). Thus, enhancement in the photocatalytic degradation of dyes takes place.



On the basis of the above results, we propose a possible mechanism for decomposition of dyes over Ce and Mn doped TiO_2 coated CNS under visible light illumination as given in the following Eqs. (6)–(9):

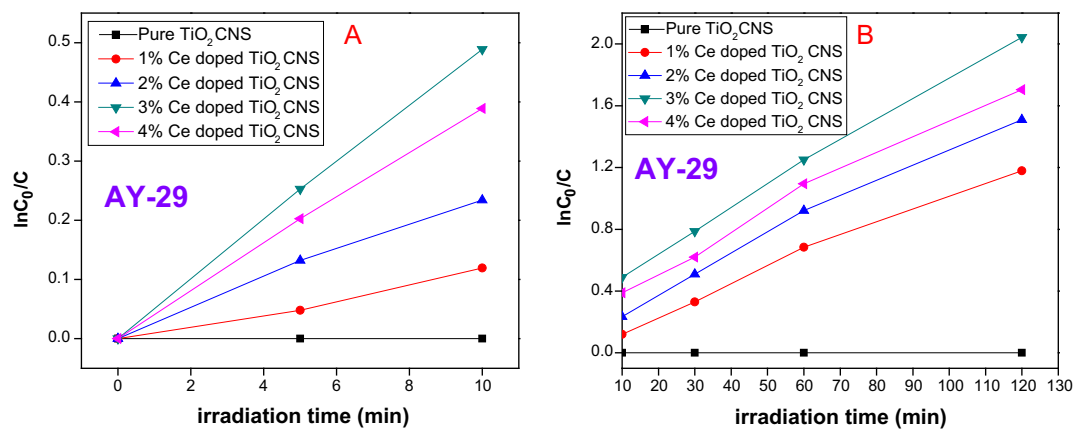


Figure 8 [A (0–10 min, B 10–120 min)] Kinetic fit for the degradation of AY-29 dye in the presence of pure and Ce-doped TiO₂ at different dopant concentration.

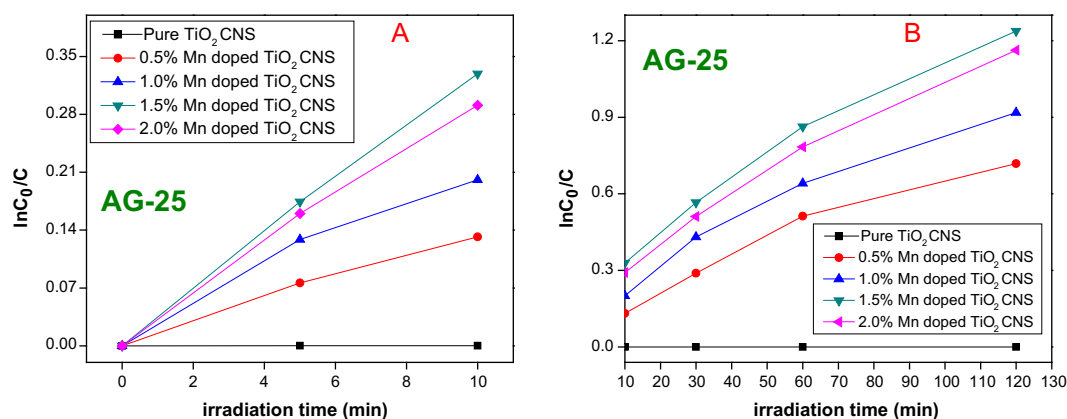
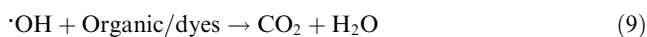


Figure 9 [A (0–10 min, B 10–120 min)] Kinetic fit for the degradation of AG-25 dye in the presence of pure and Mn-doped TiO₂ at different dopant concentration.



3.5.1. Effect of operational parameters on the decomposition efficiency of dyes

To investigate the role of active species responsible for removal of dye under visible light illumination over 3.0% Ce doped TiO₂ coated CNS (AY-29) was investigated by using different scavengers. Fig. 10 displays the change in concentration in the presence of different scavengers. In order to examine the role of hydroxyl radical we used isopropyl alcohol (IPA) as a scavenger for photodegradation of AY-29, which led to decrease in degradation rate. When potassium dichromate (PD {quencher for electron}) was added, a slight decrease in the degradation of dye take place as compared to IPA. Furthermore, the role of hole in the photodegradation of dye was determined by addition of ammonium oxalate (AO) and there was a significant reduction in decomposition process of AY-29. These

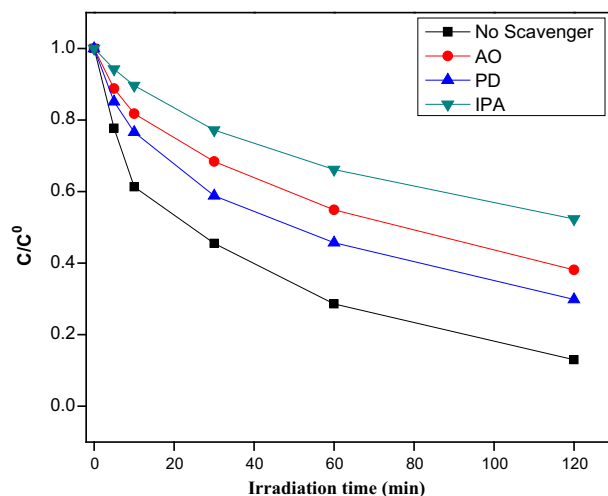


Figure 10 The effect of different scavengers on degradation of AY-29 in the presence of 3.0% Ce doped TiO₂ coated CNS under visible light illumination.

results reveal that hydroxyl radicals, electron and holes play an important role in the photodegradation of AY-29.

4. Conclusions

The photocatalytic activity of the doped TiO₂ coated CNS was studied for degradation of AY-29 and AG-25 dyes and compared with that of pure TiO₂ coated CNS. The results indicate that the doped TiO₂ was found to be more efficient for degradation of dyes under visible light source as compared to bare TiO₂. Among the doped TiO₂ 3.0% (Ce) and 1.5% (Mn) showed the highest photocatalytic efficiency. The degradation rate of dye derivatives was found to be higher for Ce-doped TiO₂ than that of Mn-doped TiO₂. The higher photocatalytic activity of Ce doped TiO₂ is due to the 4f electron transition, serving as good trapping site for an electrons. The transition of 4f electrons of Ce leads to red shift and support the separation of photogenerated electron-hole pairs which influence the degradation of the dye molecules. The XRD and Raman spectroscopic analysis of the synthesized nanospheres displays the anatase phase. The SEM image showed the spheres with rough surface, implying the deposition of Ce and Mn doped TiO₂ on the surface of carbon nanospheres. The EDX analysis also confirms the presence of dopant on the surface of TiO₂. The UV-Vis absorption spectra showed λ_{\max} shift toward longer wavelength with the increase in metal ion concentration from 1.0% to 3.0% in the case of Ce metal and 0.5–1.5% in the case of Mn metal doped TiO₂. Further increase in dopant concentration leads to decrease in λ_{\max} . At high dopant percentage the blocking of light rays or shadowing effect was observed. The turbidity of powder takes place due to aggregation of the catalyst particles, which decreases the penetration depth of light. The aggregation of TiO₂ coated CNS powder covers the part of photosensitive surface thereby decreasing the number of surface active sites. The kinetic study for degradation of dyes plays an important role for computing the efficiency viability of dye derivatives in wastewater. The prepared materials follow pseudo-first-order kinetics which was evaluated by using well known Langmuir-Hinshelwood kinetic model. The fabricated doped nanospheres showed the better antibacterial activity.

Acknowledgments

Financial support to Research Project from Ministry of Mines, Government of India, New Delhi, and Alexander von Humboldt Foundation, Germany, under research group linkage programme is gratefully acknowledged. We also thank Department of Physics and Department of Interdisciplinary Biotechnology Unit A.M.U., Aligarh, for conducting XRD-analysis and biological testing of synthesized powder.

Appendix A. Supplementary material

The method of preparation of Ce and Mn doped TiO₂ CNS and characterization using XRD, FTIR, Raman techniques and some figs showing experimental results are available.

Supplementary data associated with this article can be found, in the online version, at <http://dx.doi.org/10.1016/j.arabjc.2015.09.002>.

References

- Akpan, U.G., Hameed, B.H., 2009. Parameters affecting the photocatalytic degradation of dyes using TiO₂-based photocatalysts: a review. *J. Hazard. Mater.* 170, 520–529. <http://dx.doi.org/10.1016/j.jhazmat.2009.05.039>.
- Anil Kumar Reddy, P., Venkata Laxma Reddy, P., Maitrey Sharma, V., Srinivas, B., Kumari, V.D., Subrahmanyam, M., 2010. Photocatalytic degradation of isoproturon pesticide on C, N and S doped TiO₂. *J. Water Resour. Prot.* 02, 235–244. <http://dx.doi.org/10.4236/jwarp.2010.23027>.
- Barpuzary, D., Qureshi, M., 2013. Enhanced photovoltaic performance of semiconductor-sensitized ZnO-CdS coupled with graphene oxide as a novel photoactive material. *ACS Appl. Mater. Interf.* 5, 11673–11682. <http://dx.doi.org/10.1021/am403268w>.
- Cacho, C., Geiss, O., Barrero-Moreno, J., Binas, V.D., Kiriakidis, G., Botalico, L., Kotzias, D., 2011. Studies on photo-induced NO removal by Mn-doped TiO₂ under indoor-like illumination conditions. *J. Photochem. Photobiol. A Chem.* 222, 304–306. <http://dx.doi.org/10.1016/j.jphotochem.2011.04.037>.
- Cai, H., Liu, G., Lü, W., LI, X., YU, L., LI, D., 2008. Effect of Ho-doping on photocatalytic activity of nanosized TiO₂ catalyst. *J. Rare Earths* 26, 71–75. [http://dx.doi.org/10.1016/S1002-0721\(08\)60040-X](http://dx.doi.org/10.1016/S1002-0721(08)60040-X).
- Chand, R., Obuchi, E., Katoh, K., Luitel, H.N., Nakano, K., 2013. Effect of transition metal doping under reducing calcination atmosphere on photocatalytic property of TiO₂ immobilized on SiO₂ beads. *J. Environ. Sci.* 25, 1419–1423. [http://dx.doi.org/10.1016/S1001-0742\(12\)60211-3](http://dx.doi.org/10.1016/S1001-0742(12)60211-3).
- Chaturvedi, S.K., Ahmad, E., Khan, J.M., Alam, P., Ishtikhar, M., Khan, R.H., 2015. Elucidating the interaction of limonene with bovine serum albumin: a multi-technique approach. *Mol. Biosyst.* 11, 307–316. <http://dx.doi.org/10.1039/c4mb00548a>.
- Chowdhury, P., Moreira, J., Gomaa, H., Ray, A.K., 2012. Visible-solar-light-driven photocatalytic degradation of phenol with dye-sensitized TiO₂: parametric and kinetic study. *Ind. Eng. Chem. Res.* 51, 4523–4532. <http://dx.doi.org/10.1021/ie2025213>.
- Daghrir, R., Drogui, P., Robert, D., 2013. Modified TiO₂ for environmental photocatalytic applications: a review. *Ind. Eng. Chem. Res.* 52. <http://dx.doi.org/10.1021/ie303468t>, 130226090752004.
- Devi, L., Kumar, S., Murthy, B., Kottam, N., 2009. Influence of Mn²⁺ and Mo⁶⁺ dopants on the phase transformations of TiO₂ lattice and its photo catalytic activity under solar illumination. *Catal. Commun.* 10, 794–798. <http://dx.doi.org/10.1016/j.catcom.2008.11.041>.
- Ganesh, I., Gupta, A.K., Kumar, P.P., Sekhar, P.S.C., Radha, K., Padmanabham, G., Sundararajan, G., 2012. Preparation and characterization of Ni-doped TiO₂ materials for photocurrent and photocatalytic applications. *Sci. World J.* 2012, 1–16. [doi:10.1100/2012/127326](http://dx.doi.org/10.1100/2012/127326).
- Gogoi, S.K., Gopinath, P., Paul, A., Ramesh, A., Ghosh, S.S., Chattopadhyay, A., 2006. Green fluorescent protein-expressing *Escherichia coli* as a model system for investigating the antimicrobial activities of silver nanoparticles. *Langmuir* 22, 9322–9328. <http://dx.doi.org/10.1021/la060661v>.
- Gomez, V., Balu, A.M., Serrano-Ruiz, J.C., Irusta, S., Dionysiou, D.D., Luque, R., Santamaría, J., 2012. Microwave-assisted mild-temperature preparation of neodymium-doped Titania for the improved photodegradation of water contaminants. *Appl. Catal. A Gen.* 441–442, 47–53. <http://dx.doi.org/10.1016/j.apcata.2012.07.003>.
- Guo, L., Zhang, L., Zhang, J., Zhou, J., He, Q., Zeng, S., Cui, X., Shi, J., 2009. Hollow mesoporous carbon spheres – an excellent bilirubin adsorbent. *Chem. Commun. (Camb.)*, 6071–6073. <http://dx.doi.org/10.1039/b911083f>.

- Gurkan, Y.Y., Kasapbasi, E., Cinar, Z., 2013. Enhanced solar photocatalytic activity of TiO₂ by selenium(IV) ion-doping: characterization and DFT modeling of the surface. *Chem. Eng. J.* 214, 34–44. <http://dx.doi.org/10.1016/j.cej.2012.10.025>.
- Habib, M.A., Shahadat, M.T., Bahadur, N.M., Ismail, I.M.I., Mahmood, A.J., 2013. Synthesis and characterization of ZnO–TiO₂ nanocomposites and their application as photocatalysts. *Int. Nano Lett.* 3, 5. <http://dx.doi.org/10.1186/2228-5326-3-5>.
- Haque, M.M., Muneer, M., 2007. Photodegradation of norfloxacin in aqueous suspensions of titanium dioxide. *J. Hazard. Mater.* 145, 51–57. <http://dx.doi.org/10.1016/j.jhazmat.2006.10.086>.
- Haque, M.M., Raza, W., Khan, A., Muneer, M., 2014. Heterogeneous photocatalyzed degradation of barbituric acid and matrinidazole under visible light induced Ni, Mn, Mo and La-doped TiO₂. *J. Nanoeng. Nanomanuf.* 4, 135–139. <http://dx.doi.org/10.1166/jnan.2014.1182>.
- Jaimy, K.B., Safeena, V.P., Ghosh, S., Hebalkar, N.Y., Warriar, K.G. K., 2012. Photocatalytic activity enhancement in doped titanium dioxide by crystal defects. *Dalton Trans.* 41, 4824–4832. <http://dx.doi.org/10.1039/c2dt12018f>.
- Jiang, X., Yang, L., Liu, P., Li, X., Shen, J., 2010. The photocatalytic and antibacterial activities of neodymium and iodine doped TiO₂ nanoparticles. *Colloids Surf. B Biointerf.* 79, 69–74. <http://dx.doi.org/10.1016/j.colsurfb.2010.03.031>.
- Josset, S., Keller, N., Lett, M.-C., Ledoux, M.J., Keller, V., 2008. Numeration methods for targeting photoactive materials in the UV-A photocatalytic removal of microorganisms. *Chem. Soc. Rev.* 37, 744–755. <http://dx.doi.org/10.1039/b711748p>.
- Kuyumcu, Ö.K., Kibar, E., Dayıoğlu, K., Gedik, F., Akın, A.N., Özkara-Aydinoğlu, Ş., 2015. A comparative study for removal of different dyes over M/TiO₂ (M = Cu, Ni Co, Fe, Mn and Cr) photocatalysts under visible light irradiation. *J. Photochem. Photobiol. A Chem.* 311, 176–185. <http://dx.doi.org/10.1016/j.jphotochem.2015.05.037>.
- Li, H., Wang, G., Zhang, F., Cai, Y., Wang, Y., Djerdj, I., 2012. Surfactant-assisted synthesis of CeO₂ nanoparticles and their application in wastewater treatment. *RSC Adv.* 2, 12413. <http://dx.doi.org/10.1039/c2ra21590j>.
- Li, M., Li, W., Liu, S., 2011. Hydrothermal synthesis, characterization, and KOH activation of carbon spheres from glucose. *Carbohydr. Res.* 346, 999–1004. <http://dx.doi.org/10.1016/j.carres.2011.03.020>.
- Li, X., Yang, Y., Yang, Q., 2013. Organo-functionalized silica hollow nanospheres: synthesis and catalytic application. *J. Mater. Chem. A* 1, 1525–1535. <http://dx.doi.org/10.1039/C2TA00077F>.
- Li, Y., Lu, G., Li, S., 2001. Photocatalytic hydrogen generation and decomposition of oxalic acid over platinumized TiO₂. *Appl. Catal. A Gen.* 214, 179–185. [http://dx.doi.org/10.1016/S0926-860X\(01\)00491-4](http://dx.doi.org/10.1016/S0926-860X(01)00491-4).
- Martins, P.M., Gomez, V., Lopes, A.C., Tavares, C.J., Botelho, G., Irusta, S., Lanceros-Mendez, S., 2014. Improving photocatalytic performance and recyclability by development of Er-doped and Er/Pr-codoped TiO₂/poly(vinylidene difluoride) – trifluoroethylene composite membranes. *J. Phys. Chem. C* 118, 27944–27953. <http://dx.doi.org/10.1021/jp509294v>.
- Matsunaga, T., Tomoda, R., Nakajima, T., Wake, H., 1985. Photoelectrochemical sterilization of microbial cells by semiconductor powders. *FEMS Microbiol. Lett.* 29, 211–214. <http://dx.doi.org/10.1111/j.1574-6968.1985.tb00864.x>.
- Nahar, M.S., Hasegawa, K., Kagaya, S., 2006. Photocatalytic degradation of phenol by visible light-responsive iron-doped TiO₂ and spontaneous sedimentation of the TiO₂ particles. *Chemosphere* 65, 1976–1982. <http://dx.doi.org/10.1016/j.chemosphere.2006.07.002>.
- Nasir, M., Xi, Z., Xing, M., Zhang, J., Chen, F., Tian, B., Bagwasi, S., 2013. Study of synergistic effect of Ce- and S-codoping on the enhancement of visible-light photocatalytic activity of TiO₂. *J. Phys. Chem. C* 117, 9520–9528. <http://dx.doi.org/10.1021/jp402575w>.
- Ni, M., Leung, M.K.H., Leung, D.Y.C., Sumathy, K., 2007. A review and recent developments in photocatalytic water-splitting using TiO₂ for hydrogen production. *Renew. Sustain. Energy Rev.* 11, 401–425. <http://dx.doi.org/10.1016/j.rser.2005.01.009>.
- Ozmen, M., Güngördü, A., Erdemoglu, S., Ozmen, N., Asilturk, M., 2015. Toxicological aspects of photocatalytic degradation of selected xenobiotics with nano-sized Mn-doped TiO₂. *Aquat. Toxicol.* 165, 144–153. <http://dx.doi.org/10.1016/j.aquatox.2015.05.020>.
- Pan, K.-Y., Chien, C.-H., Pu, Y.-C., Liu, C.-M., Hsu, Y.-J., Yeh, J.-W., Shih, H.C., 2014. Studies on the annealing and antibacterial properties of the silver-embedded aluminum/silica nanospheres. *Nanoscale Res. Lett.* 9, 307. <http://dx.doi.org/10.1186/1556-276X-9-307>.
- Paul, A.K., Prabu, M., Madras, G., Natarajan, S., 2010. Effect of metal ion doping on the photocatalytic activity of aluminophosphates. *J. Chem. Sci.* 122, 771–785. <http://dx.doi.org/10.1007/s12039-010-0065-0>.
- Ranjit, K., Willner, I., Bossmann, S., Braun, A., 2001. Lanthanide oxide doped titanium dioxide photocatalysts: effective photocatalysts for the enhanced degradation of salicylic acid and t-cinnamic acid. *J. Catal.* 204, 305–313. <http://dx.doi.org/10.1006/jcat.2001.3388>.
- Raza, W., Haque, M.M., Muneer, M., 2014. Synthesis of visible light driven ZnO: characterization and photocatalytic performance. *Appl. Surf. Sci.* 322, 215–224. <http://dx.doi.org/10.1016/j.apsusc.2014.10.067>.
- Raza, W., Haque, M.M., Muneer, M., Fleisch, M., Hakki, A., Bahnemann, D., 2015a. Photocatalytic degradation of different chromophoric dyes in aqueous phase using La and Mo doped TiO₂ hybrid carbon spheres. *J. Alloys Compd.* 632, 837–844. <http://dx.doi.org/10.1016/j.jallcom.2015.01.222>.
- Raza, W., Haque, M.M., Muneer, M., Harada, T., Matsumura, M., 2015b. Synthesis, characterization and photocatalytic performance of visible light induced bismuth oxide nanoparticle. *J. Alloys Compd.* 648, 641–650. <http://dx.doi.org/10.1016/j.jallcom.2015.06.245>.
- Rehman, S., Ullah, R., Butt, A.M., Gohar, N.D., 2009. Strategies of making TiO₂ and ZnO visible light active. *J. Hazard. Mater.* 170, 560–569. <http://dx.doi.org/10.1016/j.jhazmat.2009.05.064>.
- Rincón, A.G., Pulgarin, C., 2003. Photocatalytic inactivation of *E. coli*: effect of (continuous-intermittent) light intensity and of (suspended-fixed) TiO₂ concentration. *Appl. Catal. B Environ.* 44, 263–284. [http://dx.doi.org/10.1016/S0926-3373\(03\)00076-6](http://dx.doi.org/10.1016/S0926-3373(03)00076-6).
- Rosario, A.V., Pereira, E.C., 2014. The role of Pt addition on the photocatalytic activity of TiO₂ nanoparticles: the limit between doping and metallization. *Appl. Catal. B Environ.* 144, 840–845. <http://dx.doi.org/10.1016/j.apcatb.2013.07.029>.
- Schneider, J., Matsuoka, M., Takeuchi, M., Zhang, J., Horiuchi, Y., Anpo, M., Bahnemann, D.W., 2014. Understanding TiO₂ photocatalysis: mechanisms and materials. *Chem. Rev.* <http://dx.doi.org/10.1021/cr5001892>.
- Shakir, M., Khan, M.S., Al-Resayes, S.I., Baig, U., Alam, P., Khan, R.H., Alam, M., 2014. In vitro DNA binding, molecular docking and antimicrobial studies on a newly synthesized poly(o-toluidine)–titanium dioxide nanocomposite. *RSC Adv.* 4, 39174. <http://dx.doi.org/10.1039/C4RA05173D>.
- Singh, H.K., Saquib, M., Haque, M.M., Muneer, M., 2007. Heterogeneous photocatalysed degradation of 4-chlorophenoxyacetic acid in aqueous suspensions. *J. Hazard. Mater.* 142, 374–380. <http://dx.doi.org/10.1016/j.jhazmat.2006.08.032>.
- Song, S., Tu, J., Xu, L., Xu, X., He, Z., Qiu, J., Ni, J., Chen, J., 2008. Preparation of a titanium dioxide photocatalyst codoped with cerium and iodine and its performance in the degradation of oxalic acid. *Chemosphere* 73, 1401–1406. <http://dx.doi.org/10.1016/j.chemosphere.2008.08.032>.

- Sreeremya, T.S., Thulasi, K.M., Krishnan, A., Ghosh, S., 2012. A novel aqueous route to fabricate ultrasmall monodisperse lipophilic cerium oxide nanoparticles. *Ind. Eng. Chem. Res.* 51, 318–326. <http://dx.doi.org/10.1021/ie2019646>.
- Štengl, V., Bakardjieva, S., 2010. Molybdenum-doped anatase and its extraordinary photocatalytic activity in the degradation of orange II in the UV and vis regions. *J. Phys. Chem. C* 114, 19308–19317. <http://dx.doi.org/10.1021/jp104271q>.
- Štengl, V., Bakardjieva, S., Murafa, N., 2009. Preparation and photocatalytic activity of rare earth doped TiO₂ nanoparticles. *Mater. Chem. Phys.* 114, 217–226. <http://dx.doi.org/10.1016/j.matchemphys.2008.09.025>.
- Titirici, M.-M., 2013. *Sustainable Carbon Materials from Hydrothermal Processes*. Wiley.
- Wang, B., Lu, X.-Y., Yu, L.K., Xuan, J., Leung, M.K.H., Guo, H., 2014. Facile synthesis of TiO₂ hollow spheres composed of high percentage of reactive facets for enhanced photocatalytic activity. *CrystEngComm* 16, 10046–10055. <http://dx.doi.org/10.1039/C4CE00826J>.
- Wang, C., Ao, Y., Wang, P., Hou, J., Qian, J., 2011. Preparation of cerium and nitrogen co-doped titania hollow spheres with enhanced visible light photocatalytic performance. *Powder Technol.* 210, 203–207. <http://dx.doi.org/10.1016/j.powtec.2011.03.015>.
- Wang, C., Ao, Y., Wang, P., Hou, J., Qian, J., 2010a. A facile method for the preparation of titania-coated magnetic porous silica and its photocatalytic activity under UV or visible light. *Colloids Surf. A Physicochem. Eng. Asp.* 360, 184–189. <http://dx.doi.org/10.1016/j.colsurfa.2010.02.030>.
- Wang, C., Ao, Y., Wang, P., Hou, J., Qian, J., 2010b. Preparation, characterization and photocatalytic activity of the neodymium-doped TiO₂ hollow spheres. *Appl. Surf. Sci.* 257, 227–231. <http://dx.doi.org/10.1016/j.apsusc.2010.06.071>.
- Wang, Z., Cai, W., Hong, X., Zhao, X., Xu, F., Cai, C., 2005. Photocatalytic degradation of phenol in aqueous nitrogen-doped TiO₂ suspensions with various light sources. *Appl. Catal. B Environ.* 57, 223–231. <http://dx.doi.org/10.1016/j.apcatb.2004.11.008>.
- Wheeler, D.A., Newhouse, R.J., Wang, H., Zou, S., Zhang, J.Z., 2010. Optical properties and persistent spectral hole burning of near infrared-absorbing hollow gold nanospheres. *J. Phys. Chem. C* 114, 18126–18133. <http://dx.doi.org/10.1021/jp1076824>.
- Xia, T., Zhang, W., Wang, Z., Zhang, Y., Song, X., Murowchick, J., Battaglia, V., Liu, G., Chen, X., 2014. Amorphous carbon-coated TiO₂ nanocrystals for improved lithium-ion battery and photocatalytic performance. *Nano Energy* 6, 109–118. <http://dx.doi.org/10.1016/j.nanoen.2014.03.012>.
- Xu, X.-H.N., Brownlow, W.J., Kyriacou, S.V., Wan, Q., Viola, J.J., 2004. Real-time probing of membrane transport in living microbial cells using single nanoparticle optics and living cell imaging. *Biochemistry* 43, 10400–10413. <http://dx.doi.org/10.1021/bi036231a>.
- Yu, J., Dai, G., Xiang, Q., Jaroniec, M., 2011. Fabrication and enhanced visible-light photocatalytic activity of carbon self-doped TiO₂ sheets with exposed {001} facets. *J. Mater. Chem.* 21, 1049–1057. <http://dx.doi.org/10.1039/C0JM02217A>.
- Yu, T., Tan, X., Zhao, L., Yin, Y., Chen, P., Wei, J., 2010. Characterization, activity and kinetics of a visible light driven photocatalyst: cerium and nitrogen co-doped TiO₂ nanoparticles. *Chem. Eng. J.* 157, 86–92. <http://dx.doi.org/10.1016/j.cej.2009.10.051>.
- Zhang, D., Li, G., Yu, J.C., 2010. Inorganic materials for photocatalytic water disinfection. *J. Mater. Chem.* 20, 4529. <http://dx.doi.org/10.1039/b925342d>.
- Zhang, Q., Wang, W., Goebel, J., Yin, Y., 2009a. Self-templated synthesis of hollow nanostructures. *Nano Today* 4, 494–507. <http://dx.doi.org/10.1016/j.nantod.2009.10.008>.
- Zhang, Y., Yuwono, A.H., Wang, J., Li, J., 2009b. Enhanced photocatalysis by doping cerium into mesoporous Titania thin films. *J. Phys. Chem. C* 113, 21406–21412. <http://dx.doi.org/10.1021/jp907901k>.
- Zhong, J., Chen, F., Zhang, J., 2010. Carbon-deposited TiO₂: synthesis, characterization, and visible photocatalytic performance. *J. Phys. Chem. C* 114, 933–939. <http://dx.doi.org/10.1021/jp909835m>.
- Zhu, J., Chen, F., Zhang, J., Chen, H., Anpo, M., 2006. Fe³⁺-TiO₂ photocatalysts prepared by combining sol-gel method with hydrothermal treatment and their characterization. *J. Photochem. Photobiol. A Chem.* 180, 196–204. <http://dx.doi.org/10.1016/j.jphotochem.2005.10.017>.